

# Signatures of two-dimensional electron gas at magnetic Heusler alloy-SrTiO<sub>3</sub> interface

P. K. Rout,<sup>1,†</sup> Himanshu Pandey,<sup>1,†</sup> Anupam,<sup>1</sup> P.

C. Joshi,<sup>1</sup> Z. Hossain,<sup>1</sup> and R. C. Budhani<sup>1,2,\*</sup>

<sup>1</sup>*Condensed Matter - Low Dimensional Systems Laboratory, Department of Physics,*

*Indian Institute of Technology Kanpur, Kanpur - 208016, India*

<sup>2</sup>*National Physical Laboratory, Council of Scientific*

*and Industrial Research, New Delhi - 110012, India*

(<sup>†</sup>P.K.R. and H.P. contributed equally to this research.)\*

(Dated: August 16, 2012)

## Abstract

We report remarkably low residual resistivity, giant residual resistivity ratio, free-electron-like Hall resistivity and high mobility ( $\approx 10^4 \text{ cm}^2\text{V}^{-1}\text{s}^{-1}$ ) charge transport in epitaxial films of Co<sub>2</sub>MnSi and Co<sub>2</sub>FeSi grown on (001) SrTiO<sub>3</sub>. This unusual behavior is not observed in films deposited on other cubic oxide substrates of comparable lattice parameters. The resistivity and Hall measurements on the films of various thickness clearly show that the extraordinary transport is attributable to a highly conducting interfacial layer. We draw a parallel between our results and the behavior of recently discovered two dimensional electron gas (2DEG) at LaAlO<sub>3</sub>/SrTiO<sub>3</sub> interface. The strong magnetic character of the Heusler alloys combined with their metallicity add a new dimension to 2DEG problem and makes it potentially important for spintronics applications.

The seemingly extraordinary electronic transport seen in epitaxial ultrathin films of  $\text{LaAlO}_3$  (LAO),  $\text{LaTiO}_3$ ,  $\text{LaVO}_3$  and related non-metallic perovskites grown on  $\text{TiO}_2$  terminated surfaces of (001) oriented  $\text{SrTiO}_3$  has taken the central stage in condensed matter physics research in recent years<sup>1-5</sup>. The origin of the two-dimensional electron gas (2DEG), whose mobility and areal density of carriers depend strongly on the growth temperature and oxygen partial pressure during growth<sup>1-4</sup>, and which can be modified further by electric field<sup>6</sup> and ultraviolet light radiation<sup>3</sup>, has been attributed to interfacial factors such as atomic relaxation, electronic reconstruction, cation intermixing and/or creation of oxygen vacancies<sup>7</sup>. The electronic properties of such interfaces have been studied extensively owing to their display of large residual resistance ratio<sup>1,8</sup>, magnetism<sup>9</sup>, two-dimensional superconductivity<sup>10,11</sup>, and quantum oscillation in the longitudinal conductivity<sup>12</sup>. While several types of oxides overlayers show unusually large interfacial conductivity<sup>8</sup>, the common denominator in all these cases is  $\text{SrTiO}_3$  (STO), which even without any overlayer but subjected to subtle surface treatments, can show fascinating 2D electronic behavior<sup>13</sup>.

Departing from the commonly used approach of growing specific oxide based overlayers, here we show, for the first time, a similar electronic transport realized at the interface of a half metallic Heusler alloy and STO. Although the origin of Heusler alloys goes as back as 1903 when the first compound  $\text{Cu}_2\text{MnAl}$  was synthesized by F. Heusler, these compounds have generated considerable interest in recent years due to a myriad of properties encompassing half metallicity combined with high Curie temperature, shape memory effect, thermoelectricity, heavy fermion superconductivity and topologically inhibited conducting states<sup>14</sup>. While our discovery of a highly conducting interface between Heusler alloys and STO can have potential technological applications, the fundamental mechanism for the origin of such a state brings into question the several interpretations given for the 2DEG in LAO/STO type of systems.

In this letter, we report the measurements of temperature dependence of electrical resistivity  $\rho(T)$ , Hall Coefficient ( $R_H$ ), and carrier mobility ( $\mu_H$ ) of thin epitaxial films of  $\text{Co}_2\text{MnSi}$  (CMS) and  $\text{Co}_2\text{FeSi}$  (CFS) grown on (001) STO. The unique features of these data are; (i) a residual resistivity ratio ( $\approx 1680$ ) comparable to that of LAO/STO system and much-much larger than that for single crystals of CFS, (ii) the  $R_H$  devoid of the characteristic anomalous behavior seen in ferromagnets and the  $R_H$  scales linearly with field as in a free electron system, (iii) a high  $\mu_H$  of  $\approx 10^4 \text{ cm}^2\text{V}^{-1}\text{s}^{-1}$ , and finally, (iv) a complete absence of these features in the films deposited under identical conditions on MgO, LAO, and  $\text{NdGaO}_3$  (NGO). Since the growth was carried out at a relatively low temperature ( $\approx 600^\circ\text{C}$ ) and under a high pressure of an inert gas, the interpretation of these results is untenable in the framework of a simple oxygen vacancy scenario. Moreover, the growth conditions used here ensured insignificant atomic migration across the interface and hence a massive doping of the STO. A plausible scenario for the electronic behavior of the interface lies in a significant band bending and formation of quantum well states at the interface, which are filled by the charge carriers migrated from the CM(F)S side.

The crystal structure of the ordered full-Heusler alloys CM(F)S consists of four *fcc* sublattices with Co atoms at  $(1/4, 1/4, 1/4)$  and  $(3/4, 3/4, 3/4)$ , the Mn (or Fe) atom at  $(0, 0, 0)$ , and the Si atom at  $(1/2, 1/2, 1/2)$  in Wyckoff coordinates. Taking advantage of the close matching of the lattice parameter with a large variety of substrates, the *Co*-based full-Heusler alloy thin films have been grown on the semiconductors and oxide dielectrics<sup>15</sup>. We have deposited a large number (over 70) of highly ordered single phase thin films of CM(F)S under various growth environments using pulsed laser ablation technique<sup>16</sup>. The substrates used for the deposition were (001) oriented LAO, MgO, NGO and STO, whose face diagonal matches quite well with the lattice parameter (approximately 0.565 nm) of CM(F)S. The growth rate of 0.0065 nm per laser pulse allows the synthesis of smooth and

uniform epitaxial films with perfect interfaces.

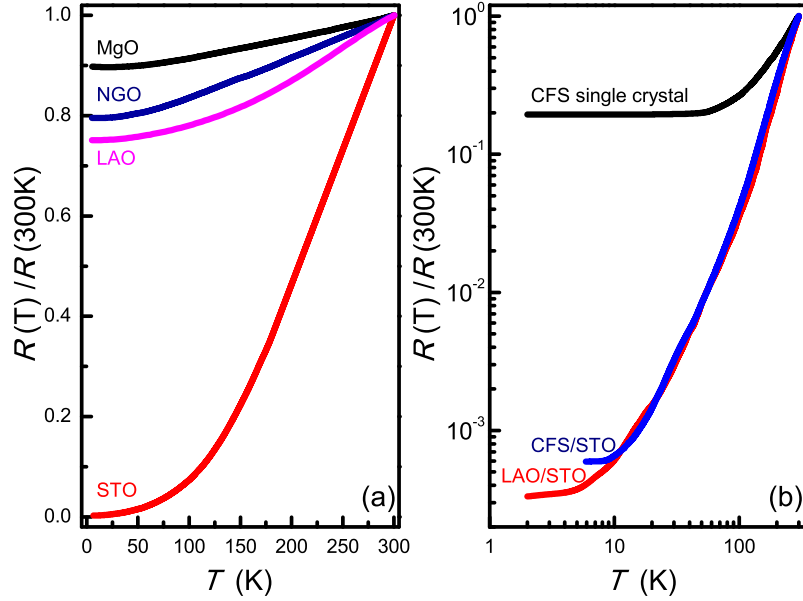


FIG. 1. (a) The normalized resistance  $R(T)/R(300\text{ K})$  of 40 nm thick CFS films on (001) oriented LAO, MgO, NGO, and STO. The films on LAO, MgO, and NGO have the residual resistivity ratio values of 1.33, 1.45, and 1.26, respectively, while for the film on STO it is  $\approx 560$ . (b) The normalized resistance for CFS single crystal<sup>18</sup>,  $\text{LaAlO}_3$  (6 nm)/ $\text{SrTiO}_3$ <sup>1</sup>, and 12 nm thick CFS on STO (Present work).

We begin by showing the most striking result of this study. Figure 1(a) compares the resistivity  $\rho(T)$  of CMS films grown on LAO, MgO, NGO, and STO at the same time. The resistivity of the films on LAO, MgO, and NGO falls by only 25% of its value at 300 K as we approach 5 K. Contrary to this, the film deposited on STO has a very low residual resistivity ( $\rho_0 \approx 0.08\ \mu\Omega\text{cm}$ ), which gives a measure of the electron scattering due to defects and impurities present in the system. Furthermore the films on STO display giant values ( $\approx 1680$ ) of residual resistivity ratio (RRR). In comparison, the lowest reported  $\rho_0$  so far for CMS films grown on any other substrate is only  $\approx 16\ \mu\Omega\text{cm}$ <sup>17</sup>. Even for the best quality single crystals, the values  $\rho_0$  are in the range of  $1.5\text{-}3.0\ \mu\Omega\text{cm}$ <sup>17,18</sup>. Similarly, the best RRR

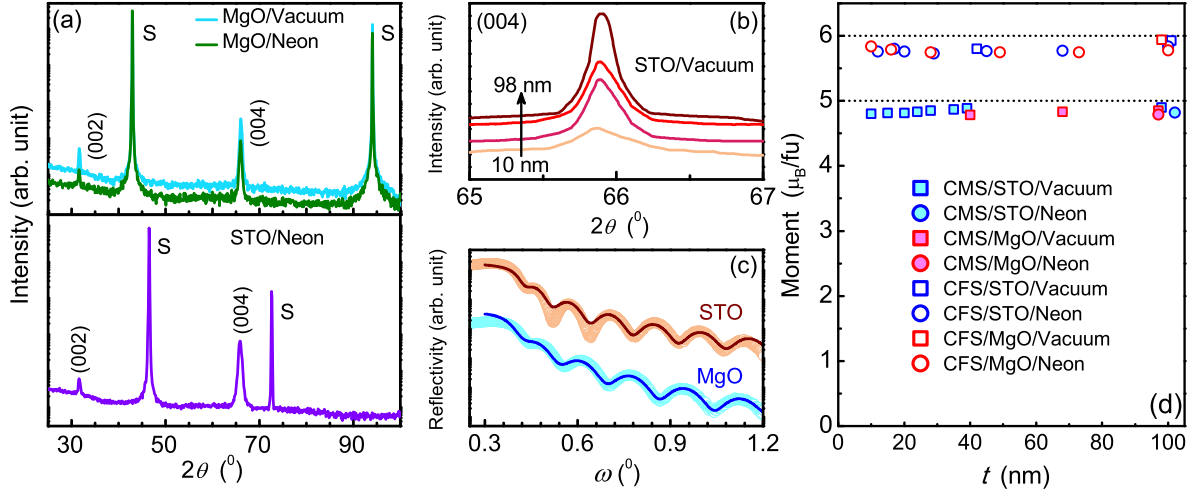


FIG. 2. (a) The  $\theta$ - $2\theta$  X-ray diffraction patterns of CFS films on MgO substrate grown in vacuum and neon (upper panel) as well as on STO in neon (lower panel). The (002) and (004) peaks of the film along with the substrate peaks are marked. (b) The small range  $\theta$ - $2\theta$  scans about (004) peak of 10, 20, 39, and 98 nm thick CMS grown on STO in vacuum. (c) X-ray reflectivity of CFS(29 nm)/STO and CMS(23 nm)/MgO films along with the fits (solid lines). (d) The variation of saturation magnetization with thickness for CMS and CFS films. These values are almost close to the Slater-Pauling values of 5  $\mu_B/\text{fu}$  and 6  $\mu_B/\text{fu}$  for CMS and CFS, respectively, shown as dotted lines.

reported for films and single crystals is limited to only 5-6<sup>17,18</sup>. The giant RRR values seen here for the films on STO are a special feature of pure defect-free samples of elemental metals like copper and gold<sup>19</sup>.

Since STO is highly prone to reduction in vacuum at elevated temperatures ( $> 850^\circ\text{C}$ ), which may render it conducting<sup>13</sup>, it is important to rule out the possibility of reduction of STO during the film growth. A bare (001) STO substrate treated under the same conditions as used for the film growth shows an insulating behavior ( $dR/dT < 0$ ) with sheet resistance of  $\approx 1 \text{ M}\Omega$  at 300 K. Furthermore, we recover the insulating nature of the STO after chemically etching off the films. A similar behavior is seen in the case where the deposition

environment was of  $3.3 \times 10^{-2}$  mbar neon. Moreover, the maximum temperature to which the substrates were exposed was limited to  $\leq 600^\circ\text{C}$  where the reduction of STO is highly unlikely<sup>13</sup>. However, the oxygen vacancies in the STO can also be created due to interfacial redox reactions with the metallic components of CM(F)S layer. But such reactions generally require a somewhat higher temperature; for example, the oxidation of Fe grown on (001) STO is only observed above  $800^\circ\text{C}$ <sup>20</sup>. A comparison of the normalized resistance of CFS/STO film with CFS single crystal and epitaxial LAO film on (001) STO provides an insight in to the origin of such low  $\rho_0$  values (See Fig. 1(b)). We can see that the resistance reduces only by a factor of  $\approx 5$  for the best quality single crystals while the same for LAO film on STO is comparable with that for CFS/STO film. One can speculate that our films behave more like a 2DEG as is the case in LAO/STO system<sup>1</sup>. However, it should be noted that the residual resistivity values of our films are two order of magnitude smaller than those for LAO/STO system<sup>21</sup>. Before making any further comparison with LAO/STO, we discuss other possible reasons which may lead to this extraordinary electronic transport seen in CM(F)S films on STO. We start by comparing the crystallographic structure and magnetic nature of these films with those deposited on MgO.

Figure 2(a,b) show the  $\theta$ - $2\theta$  X-ray diffraction profiles for CM(F)S films on MgO and STO respectively. The clear presence of the (002) and (004) reflections confirms the (00 $l$ ) oriented growth irrespective of substrate or environment. The (00 $l$ ) reflections are present even for our thinnest (10 nm) film as shown in Fig. 2(b). Moreover, the presence of the (002) peak reflects the absence of Co-Mn(Fe) antisite disorder (B2 type). The extent of  $L2_1$  ordering can be determined from the ratio of the intensities of (111) superlattice reflection and (022) fundamental reflection. We have found more than 85% ordering in our films<sup>16</sup>. Clearly, these films have high degree of crystal ordering and thus we can not expect the contrasting transport properties of the films deposited on different substrates to have any structural

root. Our X-ray data [Fig. 2(b)] reveals a maximum strain of  $-0.7\%$  for 10 nm film on STO while the thicker films undergo partial strain relaxation. It should be noted that the first principle calculations by Kandpal *et al.* show that the strains  $\leq \pm 1\%$  do not alter the band structure significantly<sup>22</sup>. Thus, the charge transport in these films should behave in the same way as that of the bulk samples. The analysis of the reflectivity curves [Fig. 2(c)] yield the root mean square interface roughness as 1-2 nm while the surface roughness is 0.8-1.4 nm, which is close to the roughness values obtained from atomic force microscopy<sup>16</sup>. Although these numbers are quite small, some interdiffusion of atoms at the CM(F)S/STO interface may still occur, which will in turn lead to doping of the STO. However, the conductivity for STO doped with the 3d-transition metal elements is quite low as compared to our values of  $\approx 8000 \text{ } \Omega^{-1}\text{cm}^{-1}$  at 300 K. For example, the 0.1 weight % of Fe doped STO has a conductivity of  $\approx 2 \times 10^{-6} \text{ } \Omega^{-1}\text{cm}^{-1}$  at 300 K<sup>23</sup>. In order to investigate this issue further, we have deposited thin films ( $\approx 60$  nm) of FeGe on (001) STO under identical conditions as used for the CM(F)S films. The sheet resistance of such films at 300 K is 1 M $\Omega$  and it diverges on cooling.

The saturation magnetic moment ( $M_S$ ) of the films grown on different substrates under identical conditions is shown in Fig. 2(d). The  $M_S$  per formula unit (fu) is  $\approx 4.9 \mu_B$  and  $\approx 5.9 \mu_B$  for our thickest CMS and CFS films, respectively. These numbers are consistent with the Slater-Pauling rule for full-Heusler alloys, i.e.  $M_s = Z - 24$ , where  $Z$  is the total number of valence electrons in the system. The value does not change much even for our thinnest film. All these results suggest that the magnetic state of our films remains invariant under the choice of the substrate and film thickness, which rules out any magnetic origin of the observed low resistivity values of the films on STO.

We believe that the explanation for the observed transport behavior of the films on STO lies in the physics and chemistry of the film-substrate interface. The role of the interface has

been examined by fabricating a series of films of varying thickness on both MgO and STO. One would anticipate that the resistivity of thinner film should be greater than that of the thicker film due to enhanced surface scattering, effects of the atomic and antisite disorder<sup>17</sup>, strain induced defects and/or the presence of electrically dead layers at the interface. Indeed, we observe such expected behavior in the films grown on MgO, where the  $\rho(T)$  increases with decreasing thickness (Fig. 3(a)). Contrary to this result, the  $\rho(T)$  of the films on STO reduces with decreasing thickness for the whole temperature range of 5-300 K (Fig. 3(b)). Clearly, this behavior indicates the presence of an electrically more conducting layer at the interface of Heusler alloy film and STO.

The conductivity of this interfacial layer can be estimated by a simple parallel resistor model, where the film is made up of a well defined interfacial layer of thickness  $t_i$  and the bulk part of film with thickness  $(t - t_i)$ . Assuming the conductivities as  $\sigma_i$  and  $\sigma_b$  for the interface and the bulk part respectively, the measured conductivity can be expressed as:

$$\sigma = \sigma_b + \frac{t_i}{t}(\sigma_i - \sigma_b) \quad (1)$$

This expression gives a linear fit of  $\sigma$  vs  $(1/t)$  curves at various temperatures. The intercept of the fits gives the values of  $\sigma_b$ , i.e.  $\sigma(t \rightarrow \infty) = \sigma_b$ . The  $\sigma_i$  can be estimated if  $t_i$  is known. Assuming the interfacial layer to be as thin as 0.5 nm, we get  $\sigma_i \approx 10^8 \Omega^{-1}\text{cm}^{-1}$  at 10 K (Fig. 3(d)). The conductivity remains at a value of  $10^7 \Omega^{-1}\text{cm}^{-1}$  even for 10 nm thick layer. While a similar large thickness of the interfacial layer has been reported in LAO/STO systems<sup>24,25</sup>, the inferred conductivity of the interface is much higher than the reported values for oxide interfaces or for doped STO at similar temperatures. For example, a conductivity of  $\sim 10^3 \Omega^{-1}\text{cm}^{-1}$  has been reported for LAO/STO<sup>24</sup> and LaTiO<sub>3</sub> (LTO)/STO<sup>11</sup> interfaces, while in case of La-doped STO, it is  $\sim 10^4 \Omega^{-1}\text{cm}^{-1}$ <sup>26</sup>.

The temperature dependence of electrical resistivity is determined by the dominant carrier



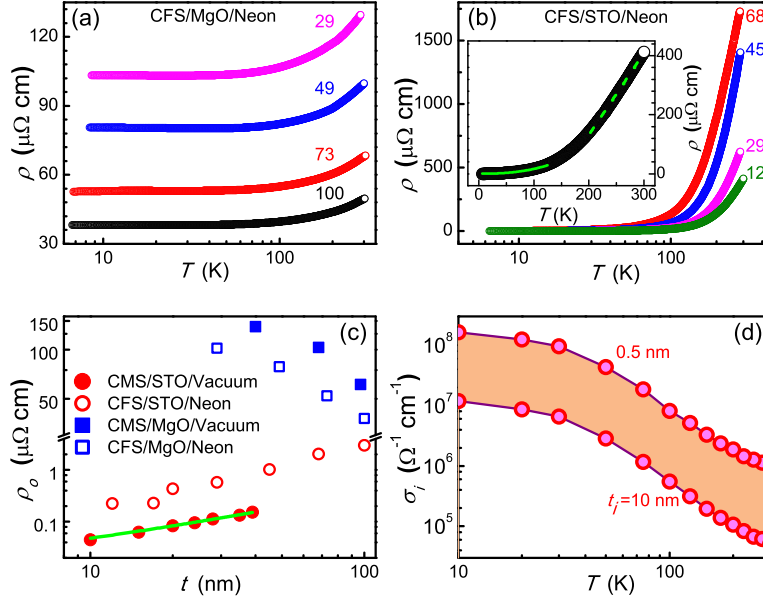


FIG. 3. The resistivity  $\rho(T)$  at different thicknesses of CFS deposited on (a) MgO and (b) STO. The thickness values are in the units of nanometers. The fits of  $\rho(T)$  data for 12 nm thick CFS/STO/Neon film using equation (2) below 125 K (solid line) and using a linear  $T$  dependence above 200 K (dashed line) are shown in the inset of (b). (c) The residual resistivity ( $\rho_0$ ) as a function of thickness. The values of  $\rho_0$  are found from the fitting of  $\rho(T)$  data by equation (2). The line shows the fit according to equation (1). (d) The temperature dependent resistivity of the interfacial layer calculated using equation (1) for two different values of interface thickness. The fitting is done on the data of CMS/STO/Vacuum films.

scattering processes in the films. We have fitted the  $\rho(T)$  for  $T \leq 125$  K curves [Fig. 3(b)] of the films grown on STO to the expression:

$$\rho(T) = \rho_0 + AT^2 + BT^3 \quad (2)$$

The  $T^2$  term is attributed to electron-electron scattering processes, which are expected in a system with partially filled  $d$ -shells of the transition metals. The coefficient of  $T^2$  term ( $A$ ) lies in the range of  $10^{-9}$ - $10^{-10}$   $\Omega\text{cmK}^{-2}$  in our films. In comparison, we found  $A \simeq 10^{-6}$

$\Omega\text{cmK}^{-2}$  for STO substrate reduced at  $800^\circ\text{C}$  for one hour in high vacuum (better than  $1.2\times 10^{-6}$  mbar), which matches quite well with the reported values of  $A$  in reduced single crystals of STO<sup>27</sup>. These observations further negate any role of oxygen deficiency in the unusual transport seen in these films. The  $T^3$  term corresponds to the unconventional one magnon scattering process due to spin fluctuations in the minority band at finite temperatures. The values of  $B$  are of the order  $10^{-11}$ - $10^{-13}$   $\Omega\text{cmK}^{-3}$ . Above  $T = 200$  K, we note that the resistivity rises linearly in temperature suggesting dominance of the electron-phonon scattering processes.

The Hall resistance ( $R_{xy}$ ) for CFS film on MgO increases with the magnetic field and then gradually saturates at higher field corresponding to the magnetic saturation field (Fig. 4(a)). This is a well know feature of ferromagnetic films, known as anomalous Hall effect. In contrast, we observe a linear field dependence of  $R_{xy}$  up to 14 T with no anomalous contribution for the films on STO. The  $R_H$  for the films on both MgO and STO is negative indicating that the charge transport is due to electron-like carriers. Figure 4(b,c) shows the carrier concentration ( $n$ ) and  $\mu_H$  of CFS/STO films as determined using the relations  $n = 1/eR_H$  and  $\sigma = ne\mu_H$ . Here the conducting layer thickness taken for these calculations is the entire thickness of the CFS film. The  $R_H$  is determined from the slope of the  $|R_{xy}|(H)$  curve for the films on STO while the slope of high field part of the curve gives  $R_H$  for the film on MgO. Although the proper understanding of  $R_H$  involves the electron like (or hole like) nature of complex Fermi surface in CM(F)S as well as the effective mass tensor for individual bands, we have assumed free electron model with single type charge carrier transport. With decreasing thickness, a monotonic increase in  $n$  is observed with a highest value of  $3.3\times 10^{21}$   $\text{cm}^{-3}$  at 2 K for 12 nm film. This can be qualitatively explained by considering the parallel

resistor model described earlier, where the Hall resistance can be expressed as:

$$R_{xy} = -\frac{B}{e\sigma^2} \left[ \left(1 - \frac{t_i}{t}\right) \sigma_b \mu_b + \frac{t_i}{t} \sigma_i \mu_i \right] \quad (3)$$

where the  $\mu_i$  and  $\mu_b$  are the mobilities of the interfacial layer and the bulk part of the film, respectively. Since  $\sigma \sim 1/t$ ,  $R_{xy} \sim t$  and thus  $n \sim 1/t$ , i. e.  $n$  increases with decreasing thickness. The thickness independence of the mobilities implies that (1)  $n \propto \sigma$  (or  $1/\rho$ ), which can be seen in the inset of Fig 4(a), and (2) the scattering due to impurities or defects does not play a dominant part in these films. We have estimated the electronic mean free path ( $l$ ) to be 2-5  $\mu\text{m}$  at 2 K from the observed values of mobility and thus a very large Ioffe-Regel parameter ( $k_F l \sim 12000 - 22000$ ). The carrier concentrations are almost independent of temperature for each thickness (Fig. 4(b)). This is in contrast to the result in LAO/STO system, where the  $n$  decreases with decreasing temperature due to the carrier freezing at the impurity sites<sup>28</sup>. On the other hand, the  $\mu_H$  decreases drastically from a very large value of  $\sim 20000 \text{ cm}^2\text{V}^{-1}\text{s}^{-1}$  at 2 K as the temperature is increased. This indicates that the low  $\rho_0$  and high RRR observed in the films are due to dominating effect of the mobility change over the corresponding change in carrier concentration. Similar high mobility charge transport has been reported for various oxide films on STO substrate like LAO<sup>1,28</sup>, SrTiO<sub>3- $\delta$</sub> <sup>13</sup>, and La-doped STO<sup>26</sup>. The  $n \approx 1.2 \times 10^{23} \text{ cm}^{-3}$  and  $\mu_H \approx 0.68 \text{ cm}^2\text{V}^{-1}\text{s}^{-1}$  of our 30 nm thick CFS film on MgO are comparable to earlier reports<sup>29</sup>. In comparison, the  $\mu_H$  in single crystal of CFS is  $\approx 35 \text{ cm}^2\text{V}^{-1}\text{s}^{-1}$ <sup>30</sup>.

All these results points towards the presence of an interfacial layer, which is at least an order of magnitude more conducting and has two orders of magnitude more mobile charge carriers as compared to the bulk values. A more intuitive interpretation of our observations can be given in terms of the strong temperature dependence of the dielectric constant ( $\epsilon$ ) of STO<sup>31</sup>, which also plays an important role in high mobility charge transport

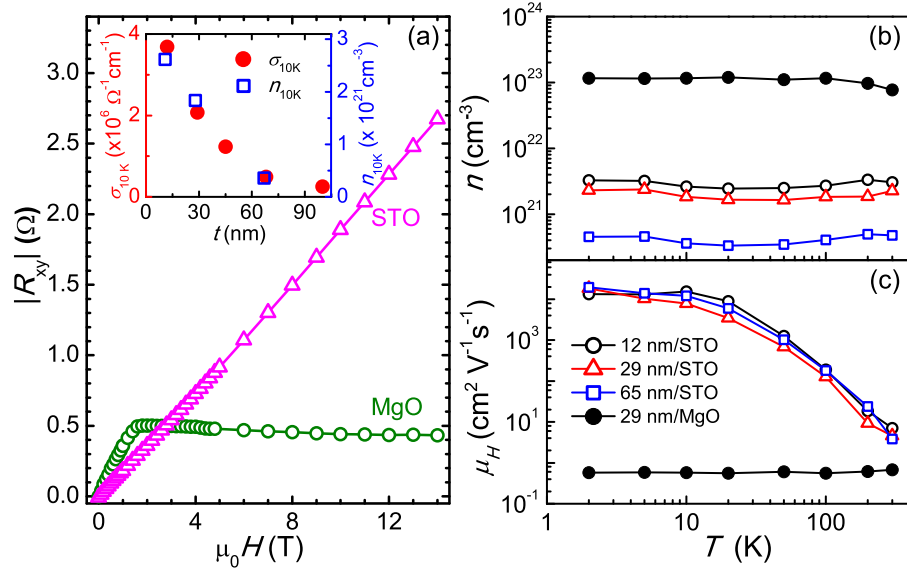


FIG. 4. (a) The Hall resistance  $|R_{xy}|(H)$  for CFS (12 nm)/STO and CFS(29 nm)/MgO films. The inset shows similarity between the thickness dependent  $\sigma$  and  $n$  data. (b) The carrier concentration ( $n$ ) for 12, 29, and 65 nm thick CFS films on STO as a function of temperature. It also shows the data for 29 nm thick CFS film on MgO. (c) The temperature dependent electron mobility ( $\mu_H$ ) of the same three films are shown in the lower panel. All the films are grown in neon environment. These measurements are performed on either the same film or simultaneously prepared films used in Fig. 3.

seen at the interface between LAO (or LTO) and STO. In LAO/STO or LTO/STO systems, the carriers induced by the polarity discontinuity at the interface introduces wedge-shaped potential, which results in STO band bending and thereby creating the interface states for the electrons<sup>11,24</sup>. We believe that, in our case, the tunneling of the carriers in to STO through the interface barrier at the interface leads to the filling of the quantum well states in the STO side of the interface.

These carriers in STO become highly mobile at low temperatures due to a diverging dielectric function which promotes charge delocalization. This explains our observation of large increase in mobility as the temperature is lowered. A greater degree of charge delocal-

ization at lower temperatures has been observed in the conductive atomic force microscopy experiments at LAO/STO interface<sup>24</sup>. The theoretical models which involve the solution of Poisson's equation with Thomas-Fermi distribution of the carriers seems to agree with this picture<sup>24,32</sup>. The Bohr radius ( $a_B$ ) determines whether the electronic correlations play a crucial role in these systems. Using the literature values of  $\epsilon \approx 330$  at 300 K (and 24123 at 4.2 K)<sup>31</sup> and the effective mass  $m^* \approx 3m_e$ <sup>25</sup>, where  $m_e$  is the electronic mass, we obtain  $a_B \approx 5.8$  nm at 300 K (and 425 nm at 4.2 K). These values are quite large compared to the electron-electron separation ( $\approx 1$  nm), which suggests the electron interactions are important for understanding of these systems.

In summary, we have observed extraordinary electron transport in epitaxial Co<sub>2</sub>MSi (M = Mn and Fe) thin films on (001) SrTiO<sub>3</sub> substrate with a low residual resistivity, which is at least an order of magnitude smaller than the values reported in these compounds so far. The films show an giant residual resistivity ratio of  $\approx 1680$  and mobility as high as  $\sim 20000$  cm<sup>2</sup>V<sup>-1</sup>s<sup>-1</sup>. The thickness dependence study establishes the presence of an electrically more conducting interfacial layer, which may be a two dimensional high mobility electron gas. The existence of such a layer opens up fresh opportunities to understand the unusual electronic behavior of perovskite oxide interfaces. The highly spin polarized character of electrons in Heusler alloys adds a magnetic dimension to the problem, which is potentially important for spintronics. Our results also bring the focus back to the origin of high mobility transport at LAO/STO interfaces and are expected to trigger research on the interfaces of several other intermetallics with SrTiO<sub>3</sub>.

The authors thank Hari Kishan, V. P. S. Awana, M. Shivkumar and the staff of Nanosciences Centre-IIT Kanpur for help in various measurements. This research has been supported by a grant from the DIT and IIT Kanpur. P.K.R. and H.P. acknowledges the financial support from the CSIR, India. R.C.B. acknowledges the J. C. Bose Fellowship

of DST.

---

\* rcb@iitk.ac.in, rcb@nplindia.org

- <sup>1</sup> A. Ohtomo and H. Y. Hwang, *Nature* **427**, 423 (2004).
- <sup>2</sup> A. Ohtomo *et al.*, *Nature* **419**, 378 (2002).
- <sup>3</sup> A. Rastogi *et al.*, *Adv. Mater.* **22**, 4448 (2010); A. Rastogi and R. C. Budhani, *Optics Letters* **37**, 317 (2012); A. Rastogi *et al.*, *Phys. Rev. B* (in press).
- <sup>4</sup> Y. Hotta, T. Susaki, and H. Y. Hwang, *Phys. Rev. Lett.* **99**, 236805 (2007).
- <sup>5</sup> S. Okamoto and A. J. Millis, *Nature* **428**, 630 (2004).
- <sup>6</sup> S. Thiel *et al.*, *Science* **313**, 1942 (2006).
- <sup>7</sup> H. Y. Hwang *et al.*, *Nat. Mat.* **11**, 103 (2012); N. Nakagawa, H. Y. Hwang, and D. A. Muller, *Nat. Mat.* **5**, 204 (2006).
- <sup>8</sup> G. Herranz *et al.*, *Phys. Rev. B* **73**, 064403 (2006).
- <sup>9</sup> L. Li *et al.*, *Nat. Phys.* **7**, 762 (2011); D. A. Dikin *et al.*, *Phys. Rev. Lett.* **107**, 056802 (2011).
- <sup>10</sup> N. Reyren *et al.*, *Science* **317**, 1196 (2007); A. D. Caviglia *et al.*, *Nature* **456**, 624 (2008).
- <sup>11</sup> J. Biscaras *et al.*, *Nat. Com.* **1**, 89 (2010); J. Biscaras *et al.*, *Phys. Rev. Lett.* **108**, 247004 (2012).
- <sup>12</sup> M. B. Shalom *et al.*, *Phys. Rev. Lett.* **105**, 206401 (2010); A. D. Caviglia *et al.*, *Phys. Rev. Lett.* **105**, 236802 (2010).
- <sup>13</sup> A. Spinelli *et al.*, *Phys. Rev. B* **81**, 155110 (2010); D. W. Reagor and V. Y. Butko, *Nat. Mat.* **4**, 593 (2005); M. Lee *et al.*, *Phys. Rev. Lett.* **107**, 256601 (2011); Y. Lee *et al.*, *Phys. Rev. Lett.* **106**, 136809 (2011).
- <sup>14</sup> T. Graf, C. Felser, and S. S. P. Parkin, *Prog. Solid State Chem.* **39**, 1 (2011).
- <sup>15</sup> K. Kasahara *et al.*, *J. Appl. Phys.* **107**, 09B105 (2010); W. H. Wang *et al.*, *Phys. Rev. B* **71**, 144416 (2005); H. Schneider *et al.*, *Phys. Rev. B* **74**, 174426 (2006); H. Pandey *et al.*, *J. Appl. Phys.* **111**, 023912 (2012); Anupam *et al.*, *J. Phys. D: Appl. Phys.* **43**, 255002 (2010).
- <sup>16</sup> See Supplemental Material.
- <sup>17</sup> M. P. Raphael *et al.*, *Phys. Rev. B* **66**, 104429 (2002).
- <sup>18</sup> C. G. F. Blum *et al.*, *Appl. Phys. Lett.* **95**, 161903 (2009).
- <sup>19</sup> M. Khoshenevisan *et al.*, *Phys. Rev. B* **19**, 3873 (1979).
- <sup>20</sup> Q. Fu and T. Wagner, *Sur. Sci. Rep.* **62**, 431 (2007).

- <sup>21</sup> G. Herranz *et al.*, Phys. Rev. Lett. **98**, 216803 (2007).
- <sup>22</sup> H. C. Kandpal *et al.*, Phys. Rev. B **73**, 094422 (2006).
- <sup>23</sup> J. Blanc and D. L. Staebler, Phys. Rev. B **4**, 3548 (1971).
- <sup>24</sup> O. Copie *et al.*, Phys. Rev. Lett. **102**, 216804 (2009).
- <sup>25</sup> A. Dubroka *et al.*, Phys. Rev. Lett. **104**, 156807 (2010).
- <sup>26</sup> J. Son *et al.*, Nature Mater. **9**, 482 (2010).
- <sup>27</sup> O. N. Tufte and P. W. Chapman, Phys. Rev. **155**, 796 (1967).
- <sup>28</sup> M. Huijben *et al.*, Nat. Mater. **5**, 556 (2006).
- <sup>29</sup> H. Schneider *et al.*, J. Phys. D: Appl. Phys. **42**, 084012 (2009).
- <sup>30</sup> We have used  $\rho = 1.5 \mu\Omega\text{cm}$ , which is the lowest value of resistivity reported in Ref. 18. The value of  $n$  is taken as  $1.2 \times 10^{23} \text{ cm}^{-3}$ , which is the value for the film on MgO.
- <sup>31</sup> R. C. Neville, B. Hoeneisen, and C. A. P. Mead, J. Appl. Phys. **43**, 2124 (1972).
- <sup>32</sup> W. Siemons *et al.*, Phys. Rev. Lett. **98**, 196802 (2007).

## SUPPLEMENTAL MATERIAL

### Film Deposition

The epitaxial thin films of Heusler alloys  $\text{Co}_2\text{MnSi}$  and  $\text{Co}_2\text{FeSi}$  were grown on (001) oriented  $\text{LaAlO}_3$  (LAO),  $\text{MgO}$ ,  $\text{NdGaO}_3$  (NGO), and  $\text{SrTiO}_3$  (STO) single crystal substrates by pulsed laser deposition technique using a KrF excimer laser ( $\lambda = 248$  nm) from stoichiometric targets in an all-metal-seal high vacuum chamber equipped with a Ti-getter pump, and an ultrahigh vacuum compatible substrate heater, which could heat the samples to  $850^\circ\text{C}$ . The laser fluency of  $\approx 3 \text{ Jcm}^{-2}$  enabled a slow growth rate of  $0.0065 \text{ nm}$  per pulse. We have deposited the films under two different conditions: in high vacuum ( $< 1.2 \times 10^{-6}$  mbar), and in an optimized neon pressure of  $3.3 \times 10^{-2}$  mbar. For the films deposited in vacuum, we have used a growth temperature of  $200^\circ\text{C}$  followed by one hour annealing at  $600^\circ\text{C}$  to enhance crystallization and ordering in the films. On the other hand, the films in neon have been deposited at  $600^\circ\text{C}$  and no post-deposition annealing was done.

### Structural Characterization

Substrate $a_{sub}$ (nm)		Misfit (%)	Strain
LAO	0.3780	5.8	Compressive
NGO	0.3863	3.5	Compressive
STO	0.3905	2.4	Compressive
MgO	0.4211	-5.0	Tensile

TABLE I. Lattice misfit between CMS and different substrates. Here the lattice misfit is defined as  $(a_{CMS} - \sqrt{2}a_{sub})/\sqrt{2}a_{sub}$ , where  $a_{CMS} = 0.5655 \text{ nm}$  and  $a_{sub}$  are the lattice parameters of CMS and substrate, respectively. The misfits are almost identical for CFS as  $a_{CFS} \approx a_{CMS}$ .

Table 1 shows the lattice misfit of CM(F)S with LAO, NGO, STO, and MgO. The face



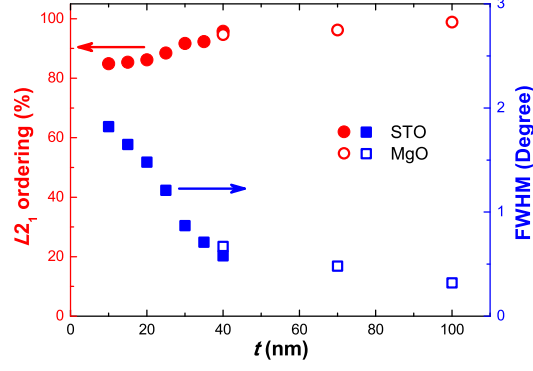


FIG. 5. The  $L_{21}$  ordering and FWHM of (004) reflection for CMS films on MgO and STO as a function of thickness. Although the ordering decreases with decreasing thickness, it is more than 85% for all the films. The FWHM increases with decreasing thickness and the corresponding crystallite size decreases from 30 nm to 5 nm.

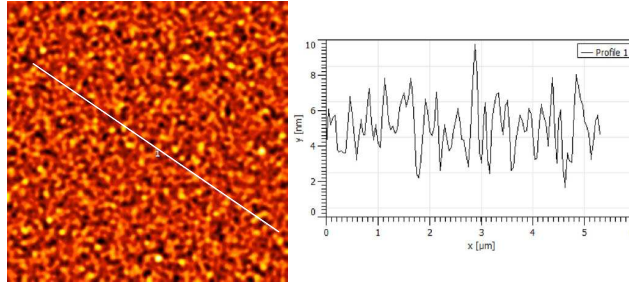


FIG. 6. A  $5 \times 5 \mu\text{m}^2$  AFM image of CFS (29 nm)/STO film along with a line scan.

diagonal of substrates matches quite well with the lattice parameter of CM(F)S with the misfits lying within 6%. While the films on MgO is under an in-plane tensile strain, the compressive strain is observed for the films on other three substrates.

The rocking curves for the (004) reflection were measured to determine the out-of-plane mosaic spread and crystalline quality of the films. The values of the full width at half maximum (FWHM) are less than  $1.9^\circ$  even for our thinnest film of 10 nm, which indicates a strong (00 $l$ ) texturing of the films (Fig. 5). Further evidence of high quality epitaxial growth is established by four fold symmetry observed in out-of-plane  $\varphi$ -scans. We observe the film growth with the epitaxial relation [011] CM(F)S parallel to [001] direction of substrate. The

$L2_1$  ordering is determined from the intensities of (111) and (022) reflections of GIXRD curves following the procedure given by Takamura *et al.*<sup>33</sup>. Figure 6 shows a typical AFM image of our film with a root mean square roughness of 1.5 nm.

### Magnetic Characterization

The room temperature in-plane magnetic hysteresis loops are displayed in Fig. 7. The films are magnetically very soft with the coercive fields in the range of 2-7 mT. The films have almost square loops reaching saturation within 100 mT. Clearly the saturation magnetic moment remains constant irrespective of growth parameters or substrate.

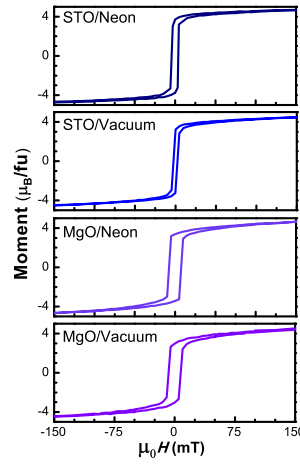


FIG. 7. The room temperature magnetic hysteresis loops, with external magnetic field ( $H$ ) applied along [110], for CMS (100 nm) films grown on MgO and STO in different environments.

### References

- [33] Y. Takamura, R. Nakane, and S. Sugahara, *J. Appl. Phys.* **105**, 07B109 (2009).